




Article

End-Region Losses in High-Power Electrical Machines: Impact of Material Thickness on Eddy Current Losses in Clamping Structures [†]

Walid Mohand Oussaid ^{1,2,*}, Abdelmounaïm Tounzi ¹, Raphaël Romary ², Abdelkader Benabou ¹,
Walid Boughanmi ³ and Daniel Laloy ³

¹ L2EP, Arts et Métiers Institute of Technology, University of Lille, Centrale Lille, Junia, ULR 2697—L2EP, 59000 Lille, France; abdelmounaim.tounzi@univ-lille.fr (A.T.); abdelkader.benabou@univ-lille.fr (A.B.)

² Laboratoire Systèmes Électrotechniques et Environnement (LSEE), University of Artois, UR 4025, 62400 Béthune, France; raphael.romary@univ-artois.fr

³ JEUMONT Electric, 59572 Jeumont, France; walid.boughanmi@jeumontelectric.com (W.B.); daniel.laloy@jeumontelectric.com (D.L.)

* Correspondence: walid.mohandoussaid@univ-lille.fr

[†] This paper is an extended version of our paper published in 2023 IEEE International Magnetic Conference—Short Papers (INTERMAG Short Papers), Sendai, Japan, 2023, pp. 1–2.

Abstract: High-power electrical machines often utilize clamping structures composed of various materials with specific geometric dimensions to secure the stator laminations. These structures are exposed to end-region magnetic flux, which induces eddy currents, leading to significant power losses that reduce the machine's efficiency. This study systematically investigates the impact of clamping plate thickness on eddy current losses across different materials and operating frequencies. A simplified experimental configuration was established to validate the numerical model developed using 3D Finite Element Method (FEM). This model was used to calculate the eddy current losses and analyze the influence of plate thickness under various conditions. A comprehensive parametric analysis was performed, revealing critical insights into the relationship between material properties, plate thickness, and loss generation. The findings indicate that while thinner plates exhibit higher current density, thicker plates provide a larger volume for current flow, resulting in varying loss patterns depending on the material's electrical and magnetic properties. The study's results offer valuable guidance for optimizing clamping structure designs in high-power electrical machines by selecting materials and thicknesses that minimize losses while maintaining mechanical integrity.

Keywords: eddy current losses; electrical machines; end-region; finite element method; clamping plates and fingers; materials for electrical machines; skin effect



Citation: Mohand Oussaid, W.; Tounzi, A.; Romary, R.; Benabou, A.; Boughanmi, W.; Laloy, D. End-Region Losses in High-Power Electrical Machines: Impact of Material Thickness on Eddy Current Losses in Clamping Structures. *Energies* **2024**, *17*, 5684. <https://doi.org/10.3390/en17225684>

Academic Editors: Dan-Cristian Popa and Emil Cazacu

Received: 30 August 2024

Revised: 6 November 2024

Accepted: 8 November 2024

Published: 14 November 2024



Copyright: © 2024 by the authors. Licensee MDPI, Basel, Switzerland. This article is an open access article distributed under the terms and conditions of the Creative Commons Attribution (CC BY) license (<https://creativecommons.org/licenses/by/4.0/>).

1. Introduction

High-efficiency electrical machines are becoming increasingly important, especially in industrial applications [1]. For an electrical machine operating on a permanent basis for a 25-year expected lifetime, energy consumption accounts for over 90% of its cost [2]. Therefore, even a minor increase in efficiency can result in substantial energy and economic savings. In accordance with IEC 60034-2-1 [3] “Standard methods for determining losses and efficiency from tests”, four distinct types of losses in rotating electrical machines are identified: copper losses in the stator and rotor conductors, iron losses in the magnetic core, mechanical losses, and additional losses, commonly referred to as stray-load losses (SLLs). Since SLLs are much more difficult to determine [4], the standard specifies different methods for measuring these losses with low, medium, or high uncertainty. In [5], the value of the stray load loss of a 200 kW cryogenic induction motor is determined by applying a factor of 1.5% of the rated output, as specified in the IEEE 112 standard. In [6],

the Finite Element Method (FEM) is employed to calculate SLL for a 500 kW induction motor. The study also provides a detailed analysis of the origin of these losses, including eddy current losses in the clamping structures. These devices are designed to secure the stator laminations in high-power electrical machines, such as large turbo-generators. They typically consist of clamping plates and fingers made of various conductive materials. They are exposed to end leakage flux generated by the currents in the stator and rotor end windings [6], which induces currents within the clamping structures. These induced currents result in additional power losses, subsequently reducing the machine's efficiency. Selecting appropriate structures and materials to minimize these losses is crucial [7]. However, accurately determining these losses is challenging due to their occurrence in regions that are not easily accessible for measurement. The quantification of such losses has then been carried out using numerical simulations on the basis of 3D FEM [7–11]. However, the majority of the studies dealt with numerical concerns such as the skin effect in the conducting surfaces where the mesh must be dense, in addition to the difficulty to account for end connections in models of large generators. Otherwise, symmetry conditions cannot be used, and model size and computation time increase rapidly. In [7], results show that using stainless steel in a 3.1 MW permanent-magnet generator reduces losses compared to construction steel, improving machine efficiency by approximately 0.075% which is significant for such machines. In order to decrease the eddy current losses in the stator-end metallic parts of a large double-canned induction motor, an arch-shaped clamping plate structure has been proposed in [8]. In [9], a calculation of eddy current losses in the plates and clamping fingers of an asynchronous machine is presented by adopting a 3D FEM with non-conformal meshing, which consists of introducing dissimilar meshes for calculating the magnetic field and current flow induced in the frequency domain. This method significantly reduces the calculation time. Further investigation into the physical aspects of the losses has been conducted to separately quantify the effect of the circumferential component of the end leakage flux on losses in the clamping devices [10]. This study reveals that the eddy currents caused by this component are very low and challenging to measure accurately. On the other hand, some studies have highlighted the sensitivity of the eddy current losses to the relative permeability value of the conducting material, hence the importance of having an accurate approximation of the $B(H)$ curve of the material [11]. In a more recent study, the work in [12] investigates the electromagnetic fields, eddy current losses, and heat transfer in the end region of a synchronous condenser, comparing different end structures and material properties. In [13], the research aims to analyze and predict the eddy current losses in generator end structures, considering multiple factors such as metal shield conductivity, relative permeability of clamping plates, and structural characteristics and using Multi-Layer Perceptron (MLP) and Support Vector Regression (SVR) techniques. Moreover, the majority of existing literature lacks comprehensive experimental validation, which is essential for confirming the accuracy of numerical models and their predictions. Exceptions include [7], which conducts efficiency measurements to validate simulation results, and [8,12,14,15], which employ temperature rise measurements as a method for experimental validation. To this end, a dedicated experimental setup is established, employing different clamping materials at various frequencies to quantify losses due to the axial component of the magnetic flux. Eddy current losses are calculated using a numerical model based on 3D FEM, and these results are compared to experimental measurements. However, the study uses the same thickness for all materials, leading to partial conclusions [16]. Typically, the sectional thickness of the clamping plate is close to one skin depth [15], but aside from mechanical considerations, the influence of clamping plate thickness on these losses has not been thoroughly investigated, even though it is well-known that the skin effect plays a crucial role in determining the depth at which currents penetrate conductive materials, particularly at higher frequencies.

In this study, a simplified configuration is utilized to perform a parametric analysis by varying the thickness of clamping plates made from different materials at multiple power supply frequencies. The aim is to investigate how eddy current losses are influenced by

both the thickness of the clamping structure and the frequency of the power supply. In contrast to our previous work in [17], this study provides experimental verification of the numerical model and a detailed, in-depth examination of the impact of clamping plate thickness on eddy current losses. The findings will provide insights into selecting clamping structures based on the material properties and their optimal thickness. The first part of the paper deals with the introduction of the test bench and its numerical model. Once the latter is validated through a comparison of the simulation results to the measurements, it is used to investigate the effects of the material thickness of the plates on the losses. This is developed in the third section, along with a discussion of the results. A conclusion is given at the end of the paper.

2. Eddy Current Loss Calculation

2.1. Experimental Bench

As demonstrated in a prior study [16], the primary source of induced currents in the end plates is the axial component of the leakage magnetic flux. Consequently, to validate the numerical model, an experimental setup is employed. It is constituted of a stator with stacked M600-65A electrical steel laminations and a clamping device. As shown in Figure 1, the latter is made up of a clamping plate and a stator sheet that supports pressure fingers made of the same material as the plate. Four distinct 15 mm-thick clamping plates and 8 mm-thick fingers, fabricated with aluminum, brass, stainless steel, and magnetic steel, are utilized, all having the same thickness. In order to focus solely on the effect of the axial component of the leakage magnetic flux, the excitation circuit consists of a circular coil constituted of a set of conductors placed above the clamping plate.

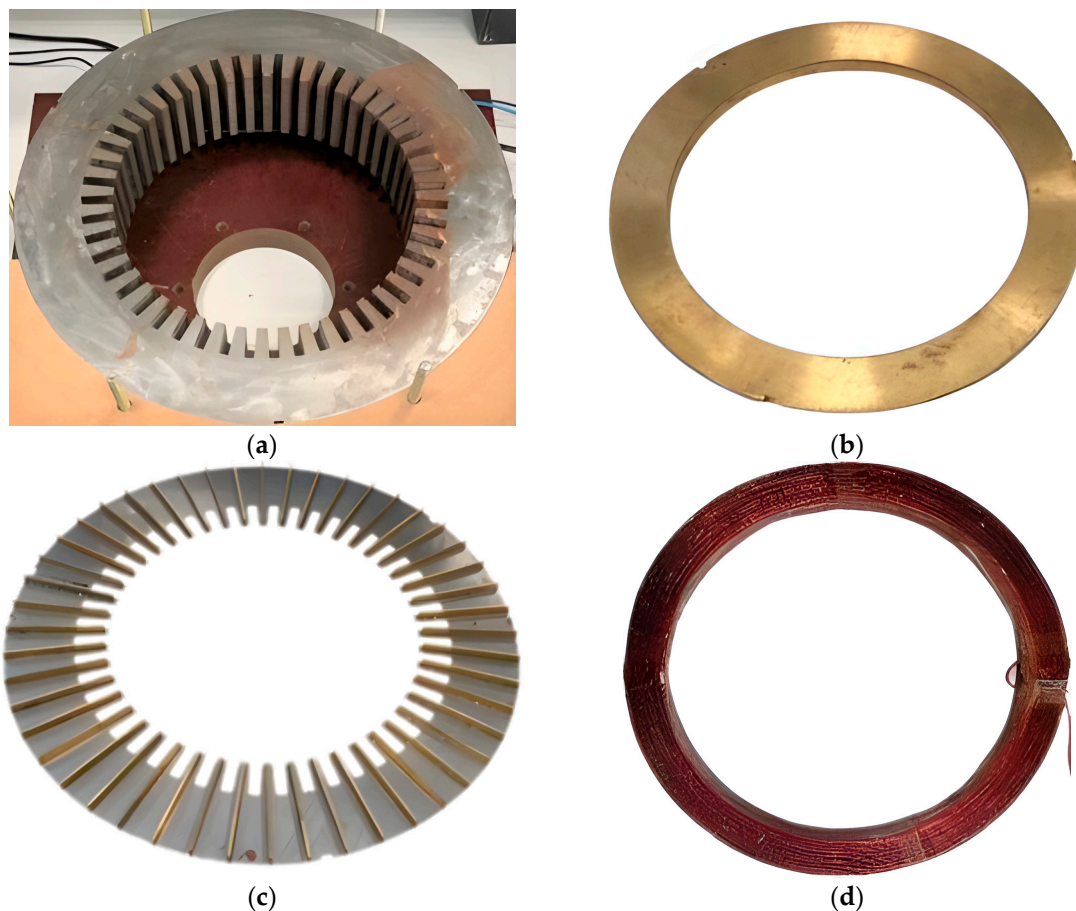


Figure 1. Different parts of the test bench: (a) the stator; (b) the clamping plate; (c) the pressure fingers; (d) the circular inductor.

A sinusoidal current at different frequencies and amplitudes supplies the coil using a programmable control voltage supply to generate a variable axial magnetic flux, which induces a current in the clamping structure. This supply is a 7kVA power amplifier, and the voltage, current, active power, and circular coil resistance are measured at the end of each test using a precision wattmeter and multimeter. The used test bench is shown in Figure 2, and its main characteristics are depicted in Table 1.

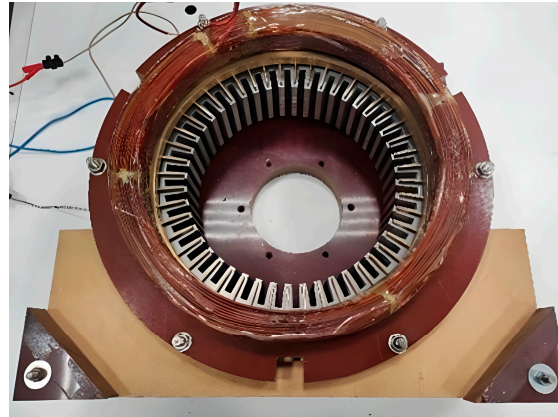


Figure 2. View of the experimental bench, from bottom to top: the stator, the pressure fingers, the clamping plate, and the circular coil.

Table 1. Characteristics of the experimental bench.

Item	Type Size
Number of slots	48
Stator inner diameter	280 mm
Stator outer diameter	460 mm
Core length	80 mm
Number of turns	175

2.2. Numerical Calculation

To calculate the eddy current losses in the clamping structure, a 3D finite element analysis (FEA) is performed using a custom 3D FEM software, *Code_Carmel* [18]. Simulations are conducted under the same conditions as the experimental tests, and the 3D AC magnetodynamic problem is resolved using the $A-\phi$ formulation in the time domain.

The relative magnetic permeabilities and electrical conductivities of the four materials at room temperature are initially determined using a mini-SST (Single Sheet Tester) device as in [19] and the four-point method [20], respectively. The resulting material properties are summarized in Table 2.

Table 2. Magnetic and electrical characteristics of the clamping plates measured in the laboratory.

Material	Relative Magnetic Permeability μ_r	Electrical Conductivity σ (MS/m)
Aluminum	1	17.93
Brass	1	15
Stainless steel	2.08	1.39
Magnetic steel	1020	6.47

For magnetic steel, the calculation is performed using the relative permeability value corresponding to the average magnetic flux density within the linear region of the $B(H)$ curve, as shown in Figure 3a. The M600-65A stator sheets were characterized using an Epstein frame in order to obtain their magnetic properties. Figure 3b shows the $B(H)$ curves of the sheets as a function of frequency, whose impact is clearly visible, as increasing it

causes a decrease in relative permeability. These curves are accurately approximated in *Code_Carmel* using an interpolation method based on spline functions [16], and they will be used for the simulations at first harmonic frequencies.

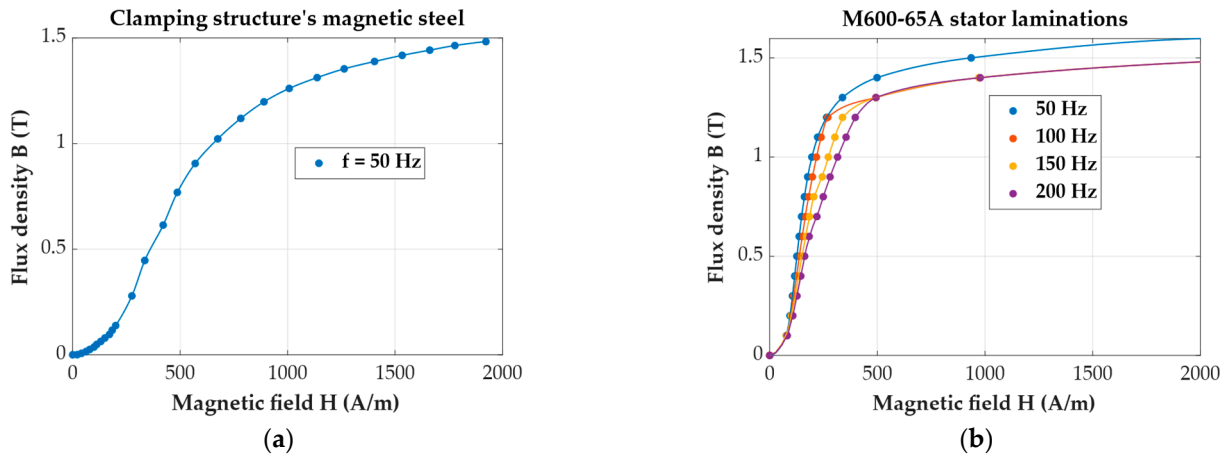


Figure 3. B(H) curves of (a) the clamping structure's magnetic steel at 50 Hz; (b) the M600-65A magnetic steel characterized using an Epstein frame.

Only a portion of the device is modeled (one slot), as depicted in Figure 4, while considering the skin effect, whose depth can be determined by the following equation:

$$\delta = \frac{1}{\sqrt{\sigma\mu\pi f}} \quad (1)$$

where σ is the electrical conductivity (S/m), μ is the magnetic permeability (H/m), and f is the power supply frequency (Hz).

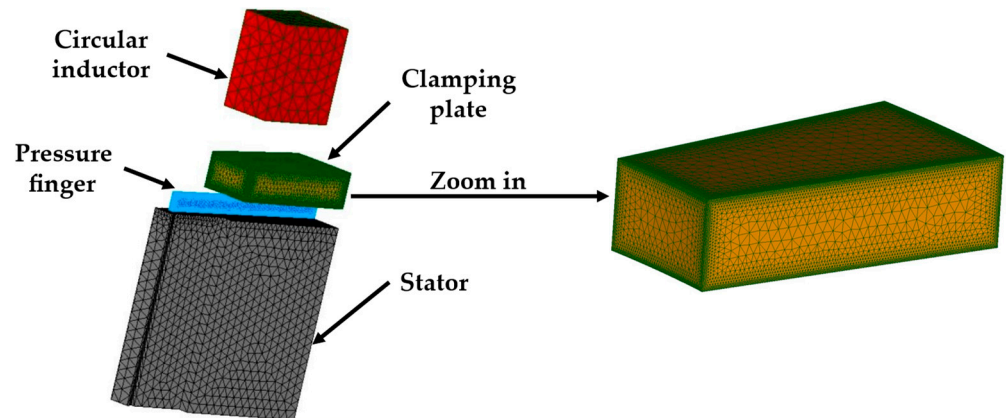


Figure 4. Mesh of the modelled system (800,000 elements).

Thus, the mesh resolution is refined to adequately address the skin effect, particularly in challenging conditions such as magnetic steel operating at 200 Hz with a skin depth of about 0.4 mm. The time step for the 3D numerical calculation is 40 points per period of the sinusoidal current signal, which corresponds to 0.5 ms at 50 Hz. Additionally, to mitigate any numerical biases, the same mesh is employed for all calculations. Concerning the boundary conditions, these are as follows:

- $B: n = 0$ in the boundary of the domain;
- $E: t = 0$ at the edges of the conducting devices;
- $J: n = 0$ on the surfaces of the pressure fingers and the clamping plate, so as to have induced currents that do not flow out of these surfaces.

The eddy current losses in the clamping system and the iron losses in the magnetic core are calculated separately, where the latter are obtained from the numerical simulation using a post-processing procedure based on Bertotti's loss decomposition [21]. It turned out that for the studied configuration and this type of excitation, the iron losses in the stator are very low and therefore can be neglected compared to the Joule losses in the circular coil. The measured active power (P_{meas}) is the sum of the resistive losses in the excitation circuit (P_J), the iron losses in the magnetic core (P_{iron}), and the eddy current losses in the clamping device (P_{eddy}):

$$P_{meas} = P_{eddy} + P_J + P_{iron} \quad (2)$$

As a consequence, the eddy current losses in the clamping plate are simply obtained in measurements by deducting the resistive losses in the circular inductor from the total measured losses. The Joule losses in the circular coil ($P_J = RI^2$) are obtained by measuring the DC resistance in this coil for each measurement point at given current and frequency using the ammeter–voltmeter method. This is completed while allowing time for thermal stabilization of the circular coil. Table 3 presents the total measured losses, eddy current losses, circular inductor resistance, and also iron losses calculation from 3D FEM for aluminum clamping structures at 50 Hz and different current amplitudes. It can be observed that the iron losses are very low and negligible. Furthermore, the resistance of the circular coil remains quasi-constant regardless of the excitation current. This is achieved by allowing the coil temperature to stabilize for each measurement point.

Table 3. Loss measurements for aluminum clamping structures at 50 Hz.

Current (A)	3	6	9	12
Measured power (W)	16.5	65.7	148.0	262.4
Eddy current losses (W)	6.6	26.1	59.0	104.2
Calculated iron losses (W)	10^{-3}	2×10^{-3}	4.5×10^{-3}	7.7×10^{-3}
Resistance (ohm)	1.0989	1.0985	1.0987	1.0984

Figures 5–8 show a comparison of the induced current losses in the clamping devices obtained from measurements and simulation for aluminum, brass, stainless steel, and magnetic steel clamping structures at 50 Hz and 200 Hz, respectively. Table 4 presents a comparison of the measured and calculated loss values for the four materials for an excitation current of 12 A at both frequencies. The results demonstrate a high degree of correlation between the measurements and the 3D FEA, with an error of less than 6% for aluminum and less than 5% for brass at both frequencies. For stainless steel, the two methods differ by 10% at 50 Hz and less than 25% at 200 Hz. The divergence between the simulation and measurement results for stainless steel, and especially for magnetic steel, may be attributed to a number of factors. These include the uncertainty in the measurement of the resistance of the circular coil, which was measured as accurately as possible as described above, as well as the uncertainty in the measurement of the electrical conductivity of the four clamping device materials. Additionally, the effect of temperature on these measured values may also contribute to the observed discrepancy. It is also important to note that the discrepancy is minimal for aluminum and brass, which are non-magnetic materials. This is why the gap is more pronounced for stainless steel and magnetic steel. Indeed, the relative permeability of stainless steel is low, making it challenging to determine accurately using a mini-SST, which is designed to characterize highly magnetic materials. In the case of magnetic steel, the calculations were based on the hypothesis of homogeneous linear permeability, which is not the case on the surface of the clamping plate due to the deterioration it may have sustained. Furthermore, as the current frequency at which the circular coil is supplied increases, the discrepancy in measurements for magnetic steel and stainless steel becomes more pronounced. This is due to the growing uncertainty in the measurement of magnetic permeability at higher frequencies.

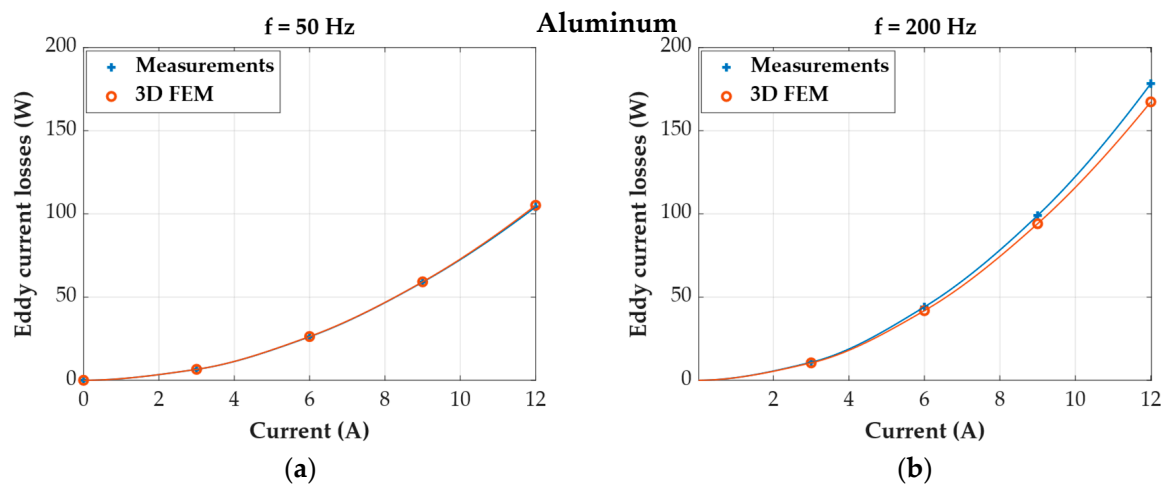


Figure 5. Measured and calculated eddy current losses in the aluminum clamping devices, where (a) at 50 Hz; (b) at 200 Hz.

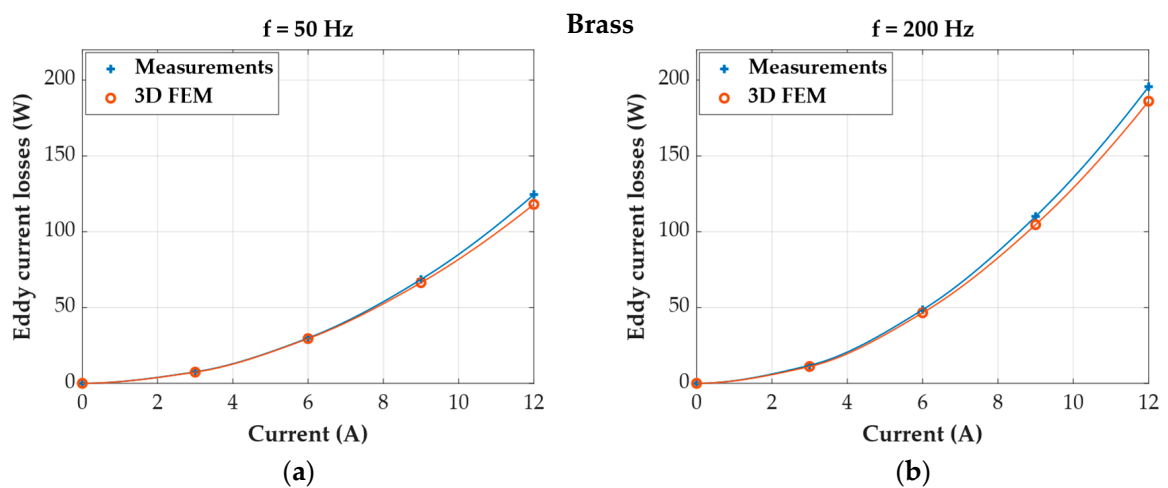


Figure 6. Measured and calculated eddy current losses in the brass clamping devices, where (a) at 50 Hz; (b) at 200 Hz.

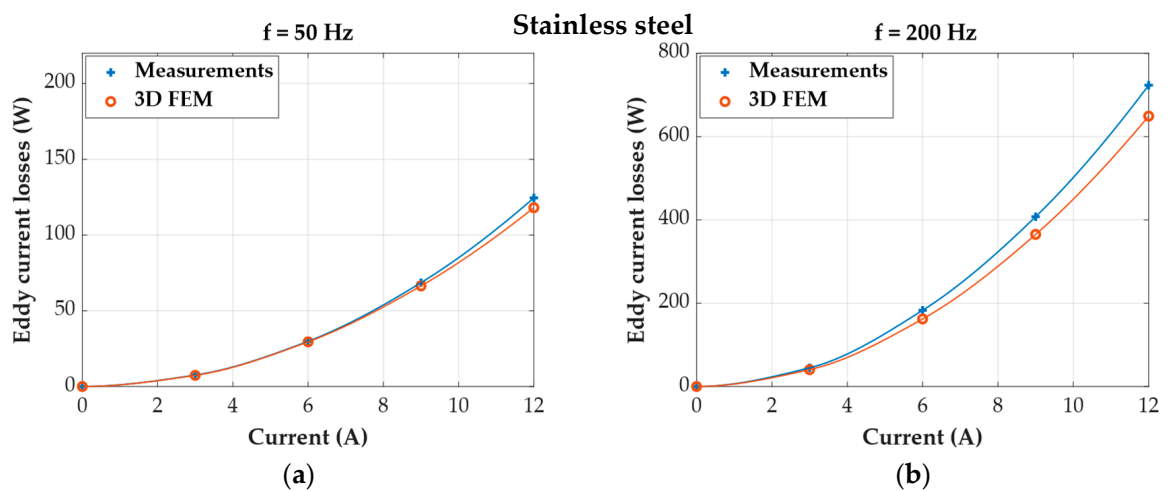


Figure 7. Measured and calculated eddy current losses in the stainless steel clamping devices, where (a) at 50 Hz; (b) at 200 Hz.

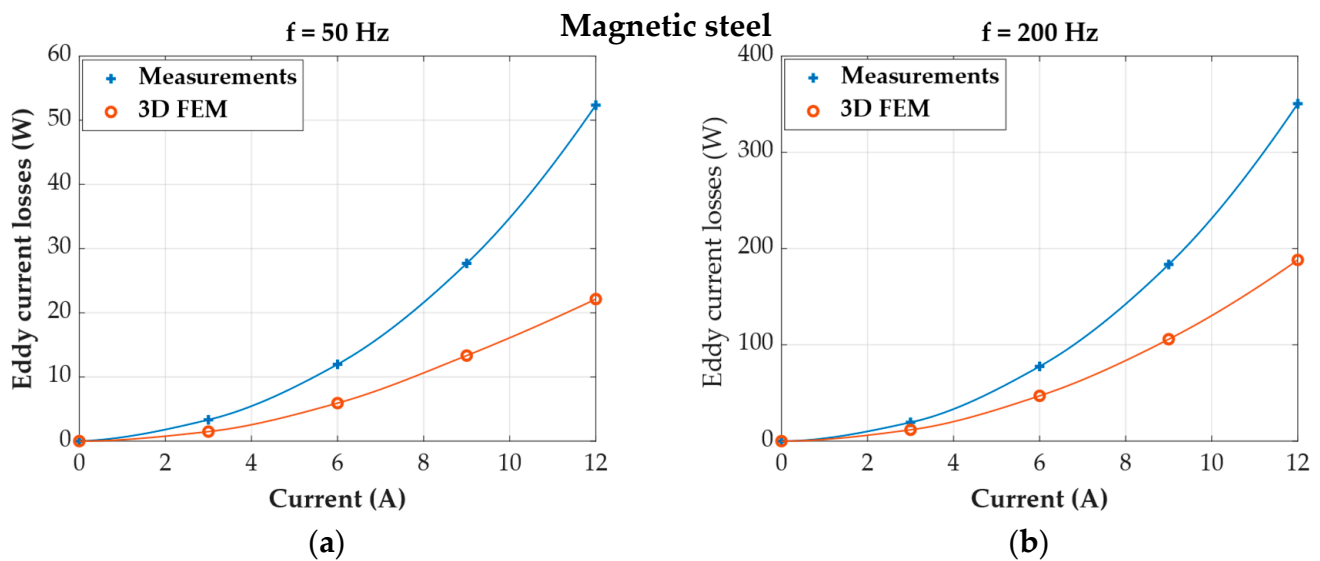


Figure 8. Measured and calculated eddy current losses in the magnetic steel clamping devices, where (a) at 50 Hz; (b) at 200 Hz.

Table 4. Comparison of the measured and calculated loss values for the four materials with an excitation current of 12 A at 50 Hz and 200 Hz.

Material	f = 50 Hz		f = 200 Hz	
	3D FEM	Test	3D FEM	Test
Aluminum	104.2	105.2	167.3	178.3
Brass	118.1	124.5	186.1	195.7
Stainless steel	87.3	115.1	649.1	723.3
Magnetic steel	22.1	52.3	188.2	350.5

When comparing losses among the four materials, we observe that losses for aluminum and brass exhibit similar behavior at both 50 Hz and 200 Hz, owing to their comparable electrical and magnetic properties. In contrast, the losses for stainless steel significantly increase at 200 Hz, surpassing those of aluminum and brass clamping structures, despite stainless steel's lower electrical conductivity. Magnetic steel losses also slightly exceed those of aluminum and brass at 200 Hz.

3. Impact of Different Quantities on Eddy Current Losses

3.1. Impact of the Stator

To analyze the effect of the stator's presence on losses caused by induced currents in the clamping devices, the same system is evaluated without the magnetic circuit. The losses are computed at 50 Hz for brass and at 200 Hz for magnetic steel clamping devices, with the results presented in Figure 9. These findings indicate that for magnetic steel and brass (and hence aluminum), the stator's effect on losses is minimal. Indeed, Figure 10 shows a field map of flux density B in the clamping plate and finger for stainless steel with and without the stator, where it can be seen that flux lines in the clamping plate are in the same direction and have equal amplitudes for both cases. While we notice a higher amplitude of flux density at the end of the pressure finger for the case where the magnetic core is present, this difference does not impact the total losses in the clamping structure as they mainly occur at the plate [16].

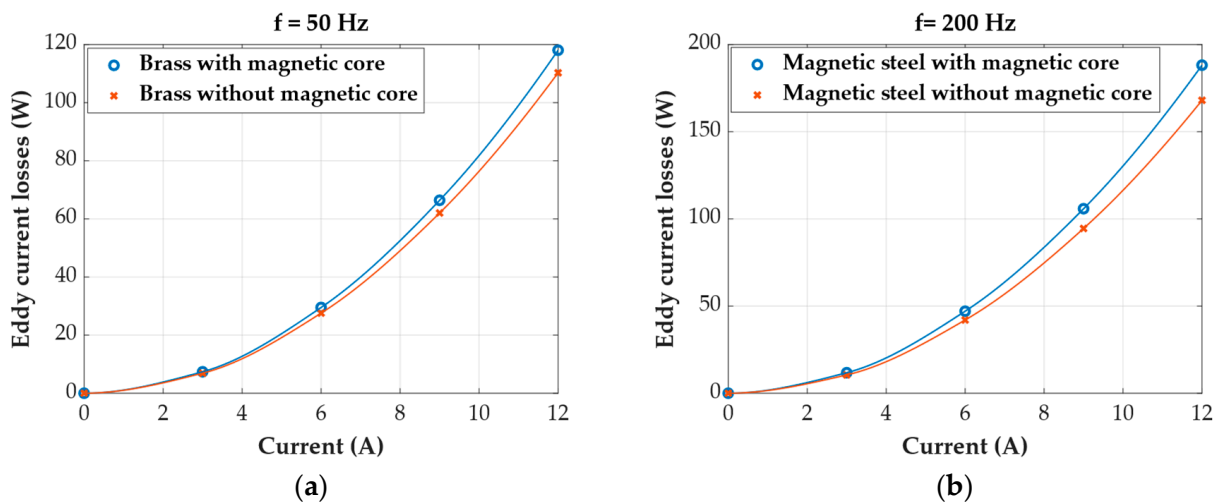


Figure 9. Comparison of eddy current losses in fingers and clamping plate with and without the magnetic core for (a) brass at 50 Hz; (b) magnetic steel at 200 Hz.

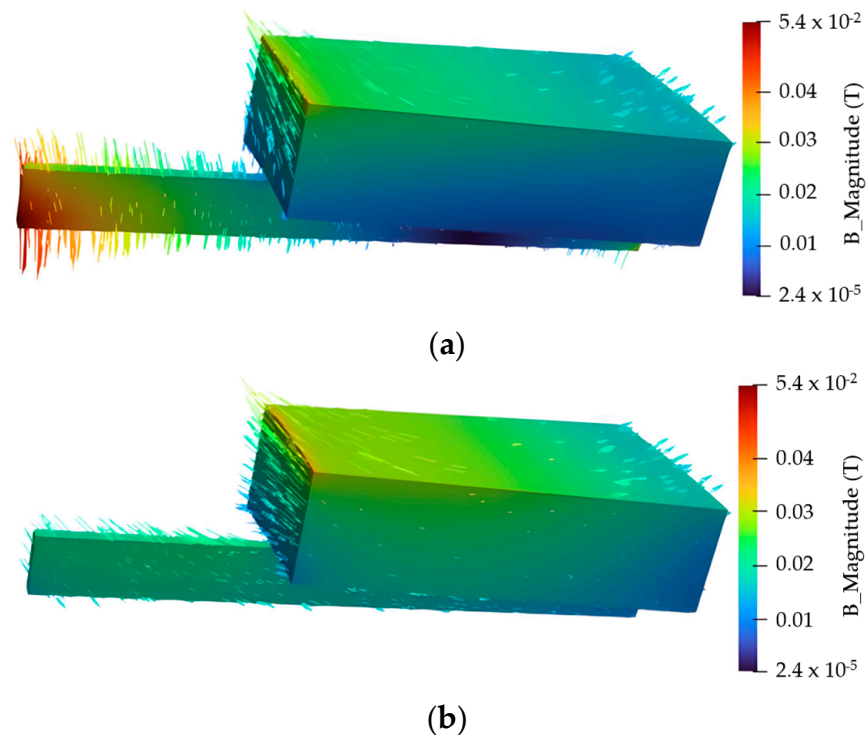


Figure 10. Flux density B (T) in the clamping plate and finger for stainless steel with (a) and without (b) the magnetic core at 50 Hz.

3.2. Impact of the Distance

Since it was found that the presence of the stator does not have a significant impact on the losses in the clamping devices, and the numerical model has been validated, the latter can be further simplified to reduce its size and thus reduce the computational time by considering a system consisting only of the clamping plate with the circular coil as shown in Figure 11. This allows us to study the effect of the plate–circular coil distance (d) on the induced current losses. Losses are calculated for an excitation current of 12 A for four different distances, from 5 mm up to 20 mm, and in particular for $d = 17$ mm to be in accordance with the distance set experimentally.



Figure 11. Experimental bench from bottom to top: the clamping plate and the circular inductor.

The same simulation conditions as the previous test bench are considered. In what follows, and as aluminum and brass have very similar magnetic and electrical properties, we will present results for aluminum, stainless steel, and magnetic steel only. Tables 5 and 6 present eddy current losses calculated as a function of the supply frequency and the distance between the clamping plate and the circular inductor (d) for aluminum, stainless steel, and magnetic steel. Obviously, the closer the plate is to the excitation source, the greater the losses are in the clamping plate for all materials. We also notice that the losses are the greatest for aluminum and the lowest for magnetic steel at 50 Hz. Meanwhile, at 200 Hz, a significant increase is noted for stainless steel compared to the other materials, and the losses in magnetic steel surpass those in aluminum. A detailed analysis of these results is provided in [16]. Given the significantly higher electrical conductivity of both aluminum and magnetic steel compared to stainless steel, it is expected that local losses would be greater in these materials. However, due to the reduced skin depth at 200 Hz, induced currents are confined to the edges of the clamping plate.

Table 5. Eddy current losses (W) in the clamping plates at 50 Hz as a function of the distance (d).

Material	Distance (mm)			
	5	10	17	20
Aluminum	138.9	120.6	100.3	93.0
Stainless steel	71.3	62.0	51.5	47.8
Magnetic steel	35.0	30.0	24.4	22.7

Table 6. Eddy current losses (W) in the clamping plates at 200 Hz as a function of the distance (d).

Material	Distance (mm)			
	5	10	17	20
Aluminum	228.5	195.7	160.9	148.7
Stainless steel	697.0	605.7	503.6	466.7
Magnetic steel	338.4	288.2	234.4	217.8

3.3. Impact of the Clamping Plate's Thickness

It can be stated that distance exerts a similar impact on losses regardless of the material utilized for the clamping devices. In order to understand the results obtained above, another aspect is the study of the impact of clamping plate material thickness on losses, by comparing this thickness with the skin depth of each material. To investigate the impact of clamping plate thickness, various thicknesses ranging from 0.8 mm to 55 mm were examined, while keeping the distance between the plate and the circular coil at 17 mm as all previous measurements and simulations had been carried out at this distance, as well as

maintaining the excitation current at 12 A. Figure 12 demonstrates the skin effect clearly in a 20 mm-thick aluminum clamping plate at 200 Hz, where the eddy current density is concentrated near the surface. In comparison, at the same thickness and material, the current flow is distributed uniformly across the entire surface of the plate at 50 Hz.

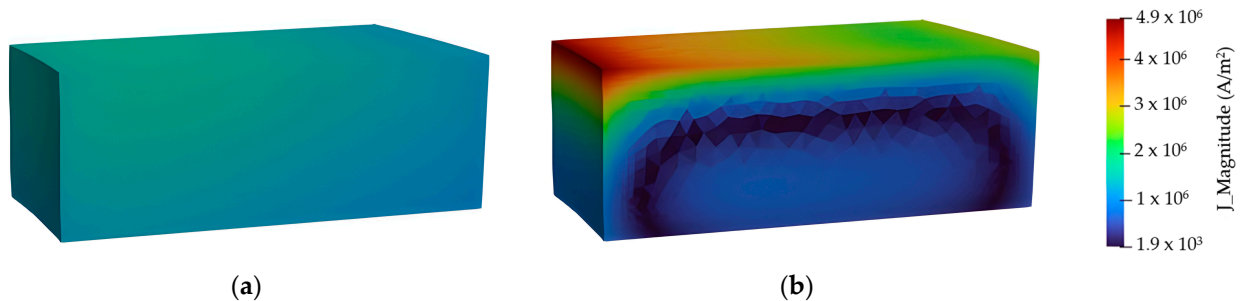


Figure 12. Eddy current density (A/m^2) for a 20 mm-thick aluminum clamping plate at (a) 50 Hz and (b) 200 Hz.

Figure 13 illustrates the distribution of eddy current density in stainless steel at 200 Hz for thicknesses of 10 mm, 20 mm, and 45 mm. The current density is prominently high and evenly spread across the plate's surface when its thickness is much less than the skin depth of stainless steel ($\delta = 24$ mm). As the plate thickness increases, maintaining the same skin depth of the material, induced currents find more volume to flow through, albeit with reduced amplitude compared to thinner plates.

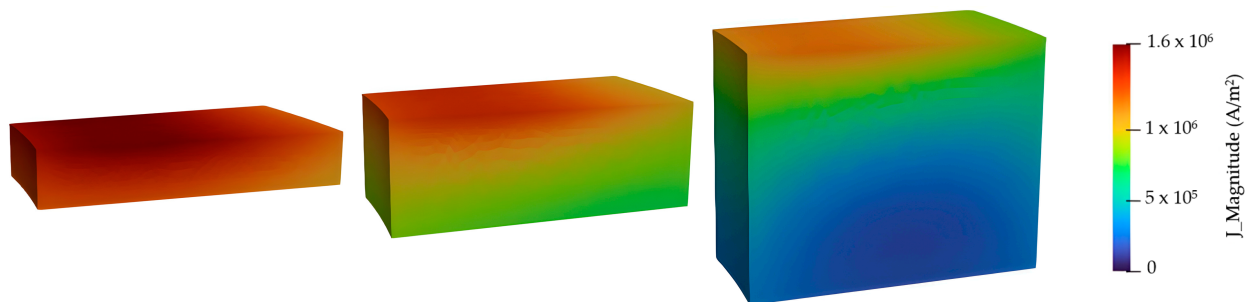


Figure 13. Eddy current density (A/m^2) for stainless steel clamping plate thicknesses of 10, 20, and 45 mm, respectively, at 200 Hz.

Figure 14 illustrates the calculated eddy current losses in the clamping plate at 50 Hz, 100 Hz, 150 Hz and 200 Hz, respectively, for the three materials. These results reveal a consistent trend for aluminum and stainless steel: losses increase with clamping plate thickness until reaching a peak at a thickness below the skin depth value. Beyond this point, losses slightly decrease and stabilize. This behavior can be explained by the current density maps, where thinner plates show high current density spread over the entire surface but with limited volume for current flow, potentially resulting in lower overall losses.

In contrast, magnetic steel exhibits relatively stable eddy current losses across varying thicknesses. This is attributed to the magnetic field and induced currents being concentrated near the surface due to the material's low skin depth at both frequencies. Consequently, increasing the thickness has minimal impact on losses.

At 150 Hz and 200 Hz, the skin depth decreases for aluminum, leading to a reduction in losses starting from thinner plates. Stainless steel, with its higher skin depth compared to other materials, shows a similar loss evolution as at 100 Hz but with a shift in the position of the peak losses. Although the mechanical aspects of clamping plates are not of interest in this work, the observation that losses evolve as a function of thickness, decreasing until they stabilize for large clamping plate thicknesses (except for magnetic steel), favors the mechanical role of clamping plates.

Globally, thinner clamping plates (<5 mm) would suggest the use of stainless steel to limit eddy current losses in the whole operating frequency range. However, this may be unsuitable in terms of mechanical strength for large electrical machines. On the other hand, for higher clamping plate thicknesses (>10 mm), magnetic steel is the best candidate for the industrial operating frequency, whereas aluminum exhibits better performances at higher operating frequencies.

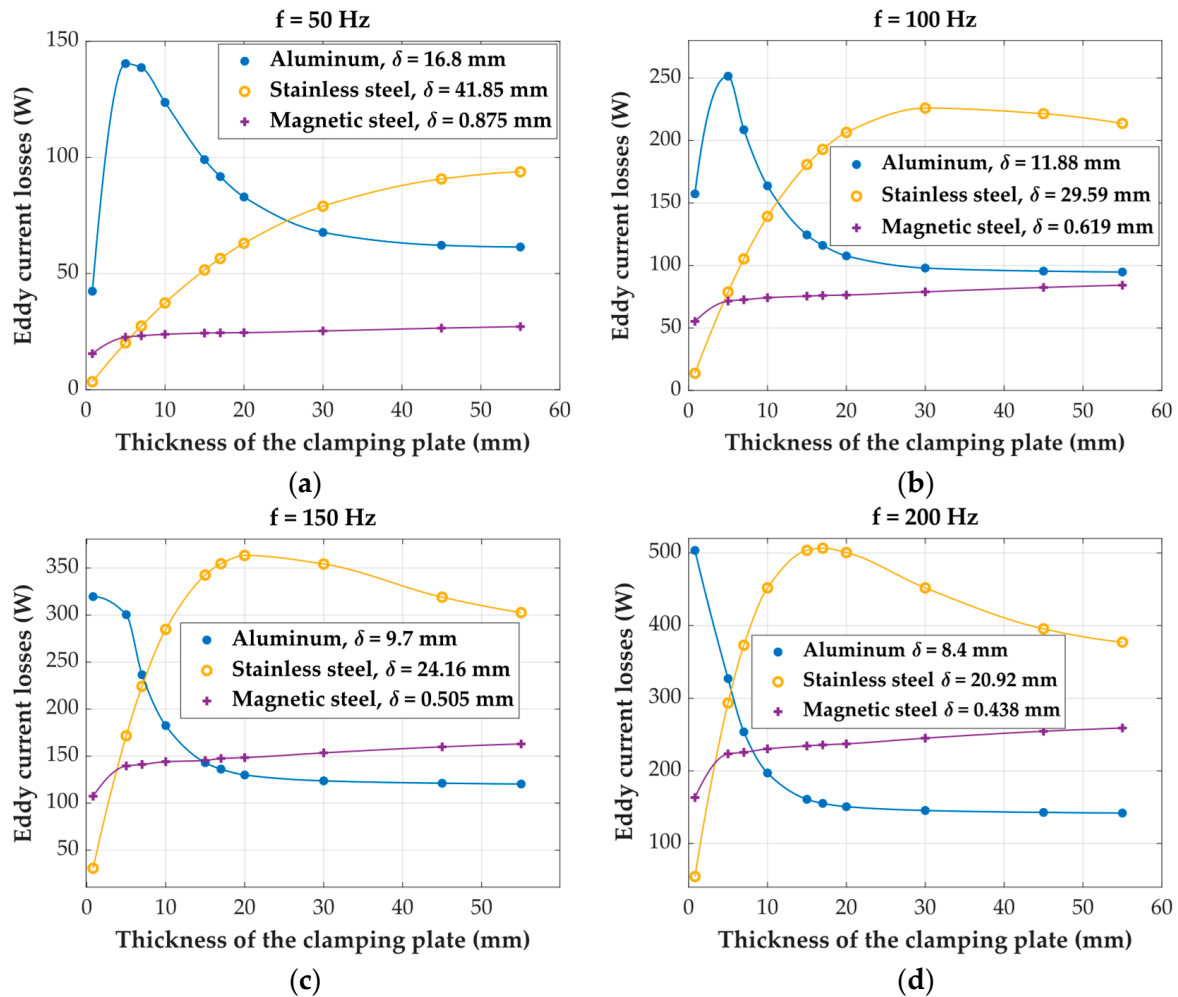


Figure 14. Eddy current losses calculated as a function of the clamping plate thickness for the three materials for an excitation current of 12 A at (a) 50 Hz; (b) 100 Hz; (c) 150 Hz; (d) 200 Hz.

4. Conclusions

This paper presented a simple and original approach to studying the effect of different clamping plate configurations on eddy current losses in high-power electrical machines. In particular, the clamping plate material as well as its thickness have been studied in terms of impact on the eddy current losses. An experimental bench has been developed to investigate the effect of the axial component of the magnetic flux on the losses in clamping devices. The effect of different clamping plate materials has been emphasized in terms of losses. For the considered experimental clamping plate thickness (15 mm), magnetic steel seems to be the best choice for a low operating frequency (50 Hz), whereas brass and aluminum have lower losses at higher frequencies (200 Hz). In addition, a numerical model has been developed and described in detail before being validated with these experimental results. Based on this numerical model, a parametric analysis of the losses in relation to the clamping plate thickness has been conducted for different materials using a less complex model that was less time-consuming to compute.

Key findings indicate that clamping plate thickness significantly affects eddy current losses, with thinner plates showing higher current densities but limited volume for current flow, while thicker plates allow for current distribution across a larger volume. However, the skin effect plays a critical role, particularly at higher frequencies, as it confines induced currents to surface regions, impacting the loss distribution. This results in varying loss patterns that depend significantly on the electrical and magnetic properties of the materials used. Furthermore, the results reveal that for materials like aluminum and brass, losses increase with thickness up to a certain point, after which they stabilize or decrease. In contrast, magnetic steel demonstrates stable losses across varying thicknesses, primarily due to its low skin depth.

These findings provide valuable guidelines for optimizing clamping structure designs, suggesting that adjusting plate thickness based on material and operating frequency can minimize eddy current losses while maintaining structural integrity.

In conclusion, this research contributes to a better understanding of how clamping plate thickness affects eddy current losses, offering practical guidance for enhancing the efficiency of high-power electrical machines through optimized design choices.

Author Contributions: Conceptualization, W.M.O., A.T., R.R. and A.B.; methodology, W.M.O., A.T., R.R. and A.B.; software, W.M.O., A.T. and A.B.; validation, W.M.O. and R.R.; formal analysis, W.M.O., A.T., R.R. and A.B.; investigation, W.M.O., A.T., R.R. and A.B.; resources, W.M.O., A.T., R.R., A.B., W.B. and D.L.; data curation, W.M.O., A.T., R.R. and A.B.; writing—original draft preparation, W.M.O.; writing—review and editing, W.M.O., A.T., R.R. and A.B.; visualization, W.M.O., A.T., R.R., A.B., W.B. and D.L.; supervision, A.T., R.R. and A.B.; project administration, A.T., R.R., A.B., W.B. and D.L.; funding acquisition, W.B. and D.L. All authors have read and agreed to the published version of the manuscript.

Funding: This research was funded by ANRT (<https://www.anrt.asso.fr/fr>, accessed on 22 August 2024).

Data Availability Statement: The original contributions presented in this study are included in the article material. Further inquiries can be directed to the corresponding author.

Acknowledgments: This work was supported by the society JEUMONT Electric, who provided the experimental bench and financial support; numerical calculations were conducted at the L2EP laboratory at Lille University; and measurements were carried out at LSEE laboratory in Artois university.

Conflicts of Interest: The authors declare no conflicts of interest.

References

1. Krings, A.; Boglietti, A.; Cavagnino, A.; Sprague, S. Soft Magnetic Material Status and Trends in Electric Machines. *IEEE Trans. Ind. Electron.* **2017**, *64*, 2405–2414. [[CrossRef](#)]
2. De Almeida, A.T.; Ferreira, F.J.T.E.; Duarte, A.Q. Technical and Economical Considerations on Super High-Efficiency Three-Phase Motors. *IEEE Trans. Ind. Appl.* **2014**, *50*, 1274–1285. [[CrossRef](#)]
3. IEC 60034-2-1: 2024; Rotating Electrical Machines—Part 2-1: Standard Methods for Determining Losses and Efficiency from Tests (Excluding Machines for Traction Vehicles). IEC: Nagoya, Japan, 2024. Available online: <https://webstore.iec.ch/en/publication/67756> (accessed on 22 August 2024).
4. Geravandi, M.; CheshmehBeigi, H.M. Stray Load Losses Determination Methods of Induction Motors-A Review. In Proceedings of the 2022 30th International Conference on Electrical Engineering (ICEE), Tehran, Iran, 17–19 May 2022; pp. 1033–1038. [[CrossRef](#)]
5. Hong, K.-P.; Lee, J. Design of 200 kW Cryogenic Induction Motor for Liquefied Natural Gas Emergency Pump. *Energies* **2024**, *17*, 1898. [[CrossRef](#)]
6. Cheaytani, J.; Benabou, A.; Tounzi, A.; Dessoude, M. Stray Load Losses Analysis of Cage Induction Motor Using 3-D Finite-Element Method with External Circuit Coupling. *IEEE Trans. Magn.* **2017**, *53*, 8202104. [[CrossRef](#)]
7. Hamalainen, H.M.; Pyrhonen, J.; Nerg, J.; Puranen, J. 3-D Finite Element Method Analysis of Additional Load Losses in the End Region of Permanent-Magnet Generators. *IEEE Trans. Magn.* **2012**, *48*, 2352–2357. [[CrossRef](#)]
8. Liang, Y.; Yu, H.; Bian, X. Finite-Element Calculation of 3-D Transient Electromagnetic Field in End Region and Eddy-Current Loss Decrease in Stator End Clamping Plate of Large Hydrogenerator. *IEEE Trans. Ind. Electron.* **2015**, *62*, 7331–7338. [[CrossRef](#)]
9. Stermecki, A.; Biro, O.; Bakhsh, I.; Rainer, S.; Ofner, G.; Ingruber, R. 3-D Finite Element Analysis of Additional Eddy Current Losses in Induction Motors. *IEEE Trans. Magn.* **2012**, *48*, 959–962. [[CrossRef](#)]

10. Darques, K.; Tounzi, A.; Benabou, A.; Shihab, S.; Korecki, J.; Boughanmi, W.; Laloy, D. Iron loss quantification in the aim of the estimation of eddy currents in clamping devices. *Eur. J. Electr. Eng.* **2021**, *23*, 481–486. [[CrossRef](#)]
11. Waldhart, F.J.; Bacher, J.P.; Maier, G. Modeling eddy current losses in the clamping plate of large synchronous generators using the finite element method. In Proceedings of the International Symposium on Power Electronics, Electrical Drives, Automation and Motion, Sorrento, Italy, 20–22 June 2012; pp. 1468–1473. [[CrossRef](#)]
12. Bi, X.; Wang, L.; Marignetti, F.; Zhou, M. Research on Electromagnetic Field, Eddy Current Loss and Heat Transfer in the End Region of Synchronous Condenser with Different End Structures and Material Properties. *Energies* **2021**, *14*, 4636. [[CrossRef](#)]
13. Wang, L.; Sun, Y.; Kou, B.; Bi, X.; Guo, H.; Marignetti, F.; Zhang, H. Prediction of Electromagnetic Characteristics in Stator End Parts of a Turbo-Generator Based on MLP and SVR. *Energies* **2021**, *14*, 5908. [[CrossRef](#)]
14. Wang, L.; Li, W. Assessment of the Stray Flux, Losses, and Temperature Rise in the End Region of a High-Power Turbogenerator Based on a Novel Frequency-Domain Model. *IEEE Trans. Ind. Electron.* **2018**, *65*, 4503–4513. [[CrossRef](#)]
15. Holland, S.A. Three dimensional finite element analysis of stator clamp plate losses of large turbo-generators. In Proceedings of the 2002 International Conference on Power Electronics, Machines and Drives (Conf. Publ. No. 487), Sante Fe, NM, USA, 4–7 June 2002; pp. 586–591. [[CrossRef](#)]
16. Mohand Oussaid, W.M.A.; Tounzi, A.; Romary, R.; Benabou, A.; Laloy, D.; Boughanmi, W. Investigation of Losses in Fingers and Clamping Plates of High-Power Electrical Machines. In Proceedings of the 2022 International Conference on Electrical Machines (ICEM), Valencia, Spain, 5–8 September 2022; pp. 2187–2192. [[CrossRef](#)]
17. Mohand Oussaid, W.M.A.; Tounzi, A.; Romary, R.; Benabou, A.; Laloy, D.; Boughanmi, W. Influence of Thickness on Eddy Current Losses in Materials Used as Clamping Structures in High-Power Electrical Machines. In Proceedings of the 2023 IEEE International Magnetic Conference—Short Papers (INTERMAG Short Papers), Sendai, Japan, 15–19 May 2023; pp. 1–2. [[CrossRef](#)]
18. Code_Carmel, LAMEL (L2EP & EDF R&D), Version 2.2.0 of 30/09/2021. Available online: <https://code-carmel.univ-lille.fr/> (accessed on 22 August 2024).
19. De Wulf, M.; Makaveev, D.; Houbaert, Y.; Melkebeek, J. Design and calibration aspects of small size single sheet testers. *J. Magn. Magn. Mater.* **2003**, *254–255*, 70–72. [[CrossRef](#)]
20. Xiong, R.; Masoumi, S.; Pakdel, A. An Automatic Apparatus for Simultaneous Measurement of Seebeck Coefficient and Electrical Resistivity. *Energies* **2023**, *16*, 6319. [[CrossRef](#)]
21. Bertotti, G. General properties of power losses in soft ferromagnetic materials. *IEEE Trans. Magn.* **1988**, *24*, 621–630. [[CrossRef](#)]

Disclaimer/Publisher’s Note: The statements, opinions and data contained in all publications are solely those of the individual author(s) and contributor(s) and not of MDPI and/or the editor(s). MDPI and/or the editor(s) disclaim responsibility for any injury to people or property resulting from any ideas, methods, instructions or products referred to in the content.